Title: Environmental fluctuations reshape an unexpected diversity-disturbance relationship in a microbial community

Authors: Christopher P. Mancuso[1], Hyunseok Lee[2], Clare I. Abreu[2], Jeff Gore[2], Ahmad S. Khalil[1,3*]

Affiliations:

[1]Department of Biomedical Engineering and Biological Design Center, Boston University, Boston, MA 02215, USA

[2]Department of Physics, Massachusetts Institute of Technology, Cambridge, MA 02139, USA

[3]Wyss Institute for Biologically Inspired Engineering, Harvard University, Boston, MA 02115, USA

*Corresponding author. Email: khalil@bu.edu (A.S.K.)

Abstract: Environmental disturbances have long been theorized to shape the diversity and composition of ecosystems. However, fundamental limitations in our ability to specify the scale and features of a disturbance in the field and laboratory have produced an inconsistent picture of diversity-disturbance relationships (DDRs). Using a recently developed automated continuous culture system, we decomposed a dilution disturbance into intensity and fluctuation components, and tested their effects on diversity of a soil-derived bacterial community across hundreds of replicate cultures. We observed an unexpected U-shaped relationship between diversity and disturbance intensity in the absence of fluctuations, counter to classic intuition. Adding fluctuations erased the U-shape and increased community diversity across all disturbance intensities. All of these results are well-captured by a Monod consumer resource model, and can be explained by a novel "niche flip" mechanism wherein tradeoffs between species growth parameters produce coexistence regimes that collapse at intermediate disturbance levels. Our results illustrate that compositional complexity of an ecosystem can be generated and predictably reshaped using temporal environmental patterns, and highlight how distinct features of disturbance can interact in complex ways to govern ecosystem assembly.

Main Text:

Biodiversity is a cornerstone of ecosystem stability and function (*1*). While it is well-appreciated that environmental changes influence species diversity in all ecosystems, the exact nature of this critical relationship is unclear. Without a predictive understanding of how ecosystems respond to perturbations, we are poorly prepared for environmental changes of anthropogenic origin, such as rising global temperatures (*2*), and unable to design effective and robust interventions in ecosystems, such as microbiomes of medical or agricultural importance (*3, 4*). Accordingly, there have been many efforts aimed at understanding the role of environmental disturbances, which reduce the biomass of a population, and various diversity-disturbance (DDR) relationships have been proposed that draw intuition from observations of natural ecosystems. A famous example is the Intermediate Disturbance Hypothesis (*5*, *6*), in which species diversity peaks at intermediate disturbance intensities (**Fig. 1A**). The basis for these relationships has long been debated, however. Earlier assertions that disturbance weakens or interrupts competition (*5*, *6*) have been refuted by both theory (*7*, *8*) and empirical findings (*9*) that harsher environments instead reinforce dependence on limiting factors.

Importantly, environmental disturbances often introduce fluctuations. The environmental fluctuations associated with a disturbance may in fact stabilize communities by creating temporal niches, similar to seasonal effects (*10*, *11*). Indeed, coexistence can be promoted in a fluctuation-dependent manner due to storage effects (e.g. dormancy in poor conditions) or if species exhibit relative non-linearities in their competitive responses (e.g. differently shaped growth curves) (*11*, *12*). Yet, coexistence might also arise from the overall time-averaged disturbance intensity in a fluctuation-independent manner (*7, 8*). To determine whether the effects of disturbance on diversity are truly fluctuation-dependent (*13*), a disturbance should be decomposed into distinct components of ***intensity*** and ***fluctuation***. Indeed, theoretical analysis has suggested that diverse DDRs can arise when considering these factors independently (*14*). Accordingly, DDRs from observational studies of disparate ecosystems and disturbance regimes often have inconsistent results (*15*, *16*). There is therefore a need for comprehensive methods and datasets that can deconvolve the effects of disturbance intensity and fluctuations.

Laboratory experiments offer a greater degree of control and throughput compared to field studies, particularly for tractable ecosystem models like microbial communities (*17*). Microbes are easily quantified with next-generation sequencing (*18–21*), and have been widely used in the laboratory to model community assembly (*22–24*), cross-feeding relationships (*25*), and succession (*26*). Laboratory models have also linked changes in diversity in response to fluctuating nutrient levels (*27*, *28*) and disturbances such as sonication (*9*), ultraviolet radiation (*29*), osmotic pressures (*12*), or toxic compounds (*30*). Dilution is perhaps the most common choice for a laboratory disturbance, as it causes species-independent mortality and replenishes the system with fresh nutrients, reminiscent of flow in soil, aquatic, or gut microbiomes. In simple batch culture experiments, where cultures sit undisturbed except for a periodic dilution step, coexistence has been observed at intermediate dilution levels (*31*, *32*), though different DDRs arise under different dilution regimes (*33*), suggesting that the dilution parameter space is vastly under-sampled. For more precise tuning of dilution or other parameters, experimentalists have long relied on continuous culture methods (*27*, *28*, *34*); unfortunately, these systems have traditionally been intractable to large-scale, multidimensional experiments. Recently, we developed eVOLVER, a flexible and automated continuous culture platform that enables independent control over conditions in a large number of mini-bioreactors (*35*, *36*), thus opening

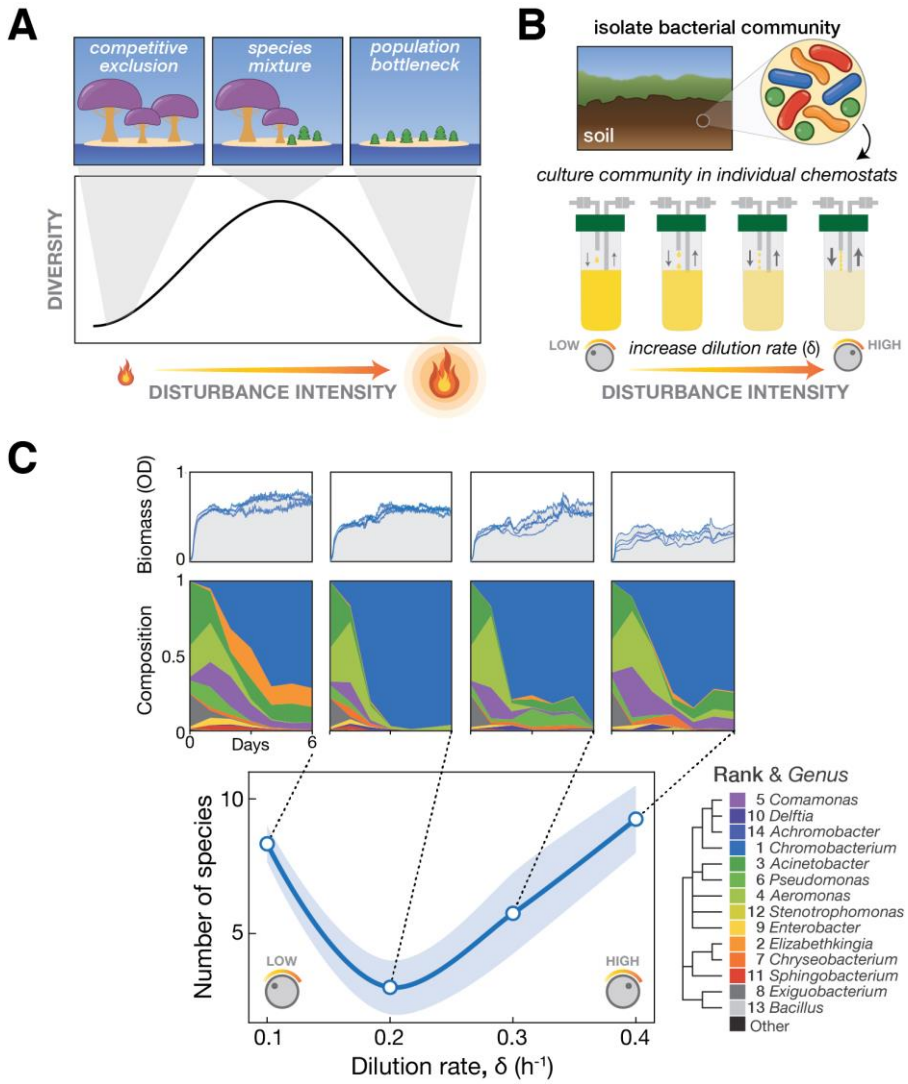

Fig. 1. Emergence of a U-shaped diversity-disturbance relationship (DDR) in a microbial community for constantly applied disturbance at different intensities. (A) DDRs have been proposed based on observations of natural ecosystems, including a classic DDR in which diversity peaks at intermediate disturbance levels. **(B)** In the laboratory, microbial communities can be cultivated and subjected to varying disturbance intensity levels by tuning the dilution rate in chemostats. **(C)** A bacterial community exhibits a U-shaped diversity dependence on the disturbance intensity. Samples of a soil-derived bacterial community were grown for 6 days in eVOLVER mini-chemostats at four different dilution rates. Top: Optical density over time quantifies biomass for replicate cultures. Middle: Mean relative abundance of bacterial genera from replicate cultures, determined by 16S sequencing. Mean rank abundance is denoted by order, taxonomic similarity is denoted by color. Bottom: Plotting the endpoint number of species (Amplicon Sequence Variants) vs. dilution rate produces a U-shaped curve, rather than a peaked DDR. Shaded window indicates a one standard deviation confidence interval.

up the possibility to explore microbial community dynamics under controlled, multidimensional environmental disturbances. By programming different dilution profiles with eVOLVER, we set out to independently quantify the effects of disturbance intensity and fluctuations on the composition and diversity of microbial communities.

First, we sought to measure microbial diversity at various levels of disturbance intensity in the absence of fluctuations. We cultivated replicate samples of a soil-derived microbiome in separate eVOLVER bioreactor arrays in dilute Nutrient Broth for six days (comprising 20-90 generations), during which continuously diluted cultures approached equilibrium. In a chemostat, the flow of media into the vessel is matched by flow of spent media and cells out of the vessel, so disturbance intensity is directly related to dilution rate (**Fig. 1B**). We thus varied the disturbance intensity by varying the dilution rate across the arrays (Materials and Methods, figs. S5 & S6). We sampled cultures daily and used 16S sequencing to quantify composition and diversity over time. As expected, we observed decreasing biomass of the cultures at increasing dilution rates (**Fig. 1C** & fig. S7**)**. Surprisingly, after quantifying the composition of each culture, we observed a U-shaped diversity-disturbance relationship (**Fig. 1C**), with the number of surviving species at intermediate dilution rate at roughly half of the number at either low or high dilution rate. This U-shape is both unexpected from classic intuition (*6*) and rare in empirical observations (*15*, *16*). Thus, to better understand our observation, we sought a modeling framework in which a U-shaped DDR could emerge under straightforward conditions of constantly applied disturbance.

We examined two broad classes of ecological models: 1) Lotka-Volterra models (*37*), in which species growth rates are a function of population size and interactions between species, and 2) consumer resource models (*38*, *39*), in which species growth rates are a function of resource concentrations. We simulated sets of 10 species, choosing growth and interaction parameter ranges that could capture the dilution experiment, as well as other biologically feasible ranges (**Materials and Methods**). In the Lotka-Volterra model, diversity was observed to decrease as a function of increasing dilution rate δ, but no U-shape was observed for a wide selection of reasonable parameter ranges (**Fig. 2A**). Turning to consumer resource models, we first simulated sets of 10 species competing for 7 resources, with per-capita growth rates composed of a sum across nutrient-specific growth rates. For a single nutrient, growth scales linearly with the concentration c according to per-resource growth rates r. Again, we did not observe a U-shaped DDR, instead observing that diversity did not vary with disturbance intensity for any of the parameter ranges tested (**Fig. 2B**). Finally, we employed a Monod growth model, in which growth rates sum across resources and saturate at high resource concentrations, with maximal growth r and half-saturation constant K. In this model, a species with high maximum growth rate r may be outcompeted at low resource levels by a species with a low saturation constant K, such that the outcome of competition varies depending on nutrient levels (and thus dilution rate). The Monod consumer resource model recapitulates the U-shaped diversity dependence on disturbance intensity that we observed in our experiments (**Fig. 2C**). We then asked whether this model could help us understand how DDRs evolve over a more comprehensive environmental disturbance parameter space.

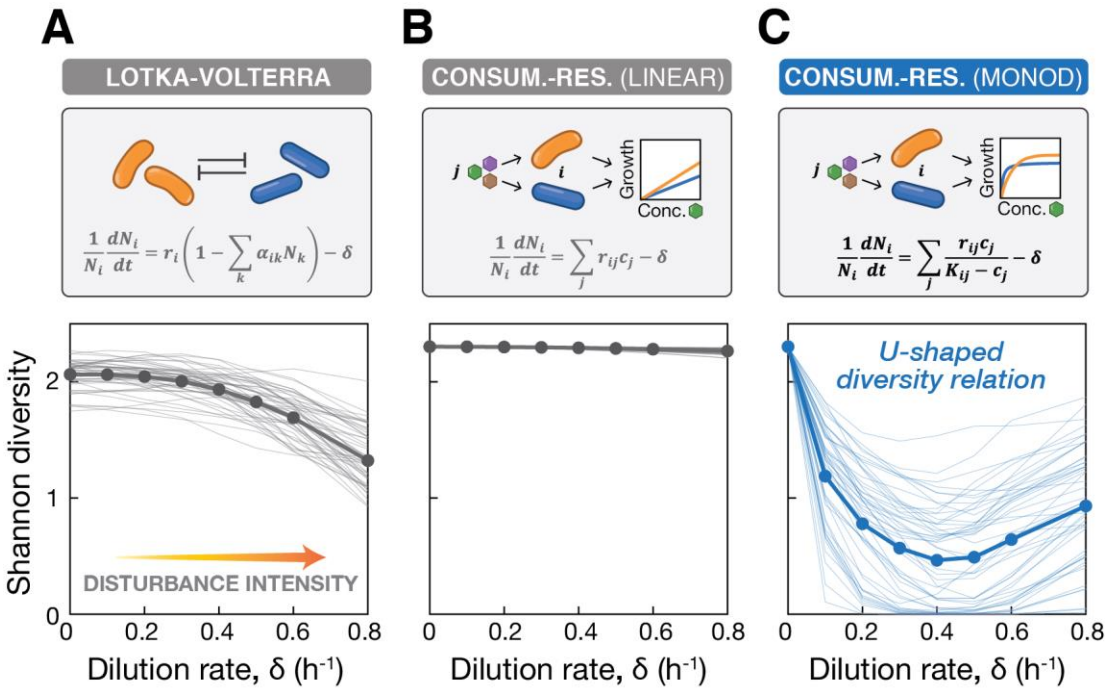

Fig. 2. A consumer resource model with Monod growth, but not other models, predicts a U-shaped diversity-disturbance intensity relationship. **(A)** Top: Lotka-Volterra model for growth of species *i* co-cultured with other species. Bottom: Shannon diversity of randomly generated 10-species communities, after six days of simulated growth at varying dilution rates. **(B)** Top: Linear consumer resource model for growth of species *i*, with additive linear growth on each resource (see inset). Bottom: Shannon diversity of randomly generated 10-species communities, after six days of simulated growth on seven resources at varying dilution rates. **(C)** Top: Monod consumer resource model for growth of species *i* with additive non-linear growth on each resource (see inset). Bottom: Shannon diversity of randomly generated 10-species communities, after six days of simulated growth on seven resources at varying dilution rates. For each model, mean diversity was computed for 100 randomly initialized communities, across each mean dilution rate, 50 of which are shown as individual traces (Materials and Methods).

Both disturbance intensity and fluctuations are hypothesized to play a role in the assembly of ecosystems, but how these two disturbance components interact to reshape DDRs is unclear. Using our modeling framework, we sought to independently vary these two components, simulating a two-dimensional dilution profile. Specifically, we introduced fluctuations into the model by permitting δ to vary with time, compressing disturbance into discrete time windows (**Fig. 3A**); this was done while keeping the time-averaged δ equal, thereby allowing us to vary disturbance intensity and fluctuation independently. The Monod consumer resource simulations predict significantly higher diversity in fluctuating conditions comprised of one or more dilution events per day (**Fig. 3D**), with the lowest-frequency (i.e. largest-fluctuation) regime predicted to maintain the most diversity. This is consistent with intuition that fluctuations introduce temporal structure into environments which may create new niches that promote diversity. Additionally, fluctuations are predicted to weaken the U-shape of the DDR, indicating that community composition is truly fluctuation-dependent in the Monod model. Conversely,

neither the Lotka-Volterra nor the linear consumer resource models predict differences in the DDR between fluctuation frequencies (figs. S8 & S9). The overlap of DDRs of different frequencies indicates that in these models the relevant metric is the time-averaged overall intensity, rather than the frequency, of disturbance (*7*, *8*).

We returned to experiments to see whether the U-shaped DDR observed in constant dilution chemostats is modulated by fluctuations, as predicted by the Monod model. To comprehensively test for fluctuation-dependency, we implemented dilution profiles with 1, 4, or 16 fluctuations per day (alongside the constant dilution conditions) at varying mean dilution rates in an eVOLVER experiment comprised of 64 simultaneous cultures ("DDR64 Experiment") (**Fig. 3B**). As before, we cultivated replicate samples of the soil-derived microbiome in eVOLVER for six days, taking samples every 24 hours to quantify composition. The specific dilution profiles we programmed were reflected in the optical density traces of each culture over time, showing differences between conditions but close agreement between replicates (**Fig. 3C** & fig. S7). Based on 16S sequencing (*18–21*), we observed that the genus-level composition of the community varied over time and between conditions (**Fig. 3D &** figs. S10 & S11). Culture compositions diverged from the initial composition, and Principle Coordinate Analysis revealed that constant dilution conditions and 1/day fluctuations diverged from each other, indicating a clear fluctuation-dependent effect, with the spread modulated by mean dilution rate (fig. S10). Notably, despite starting from a diverse community with hundreds of species, we found compositions to be largely similar between replicates (figs. S6, S10).

We calculated Shannon diversity for each timepoint (fig. S12) and found that endpoint diversity trends across disturbance intensity and fluctuation frequency are qualitatively consistent with the Monod consumer resource model in three ways (**Fig. 3E & F,** & fig. S13). 1) We observed U-shaped diversity curves in regimes of constant disturbance and small frequent disturbances, in both experiment and simulations. 2) Larger fluctuations preserved higher levels of diversity, and 3) larger fluctuations erased the U-shaped diversity curves. Our experimental results were reproducible from frozen inoculum, as confirmed by a 48-vial experiment designed to examine washout at extreme dilution rates (up to 1.5 h^{-1}) (Supplementary Note 3, & figs. S5, S10, S12, & S13). Though other measurables varied across the disturbance parameter space (e.g. biofilm, DNA content), they do not explain the differences in diversity as clearly as the Monod consumer resource model does (Supplementary Note 3, & figs. S14-16). We found it striking that the model captures the features of our results so well while being relatively simple and non-parameterized. We therefore returned to this model to uncover a potential mechanism by which the U-shaped diversity curves may emerge.

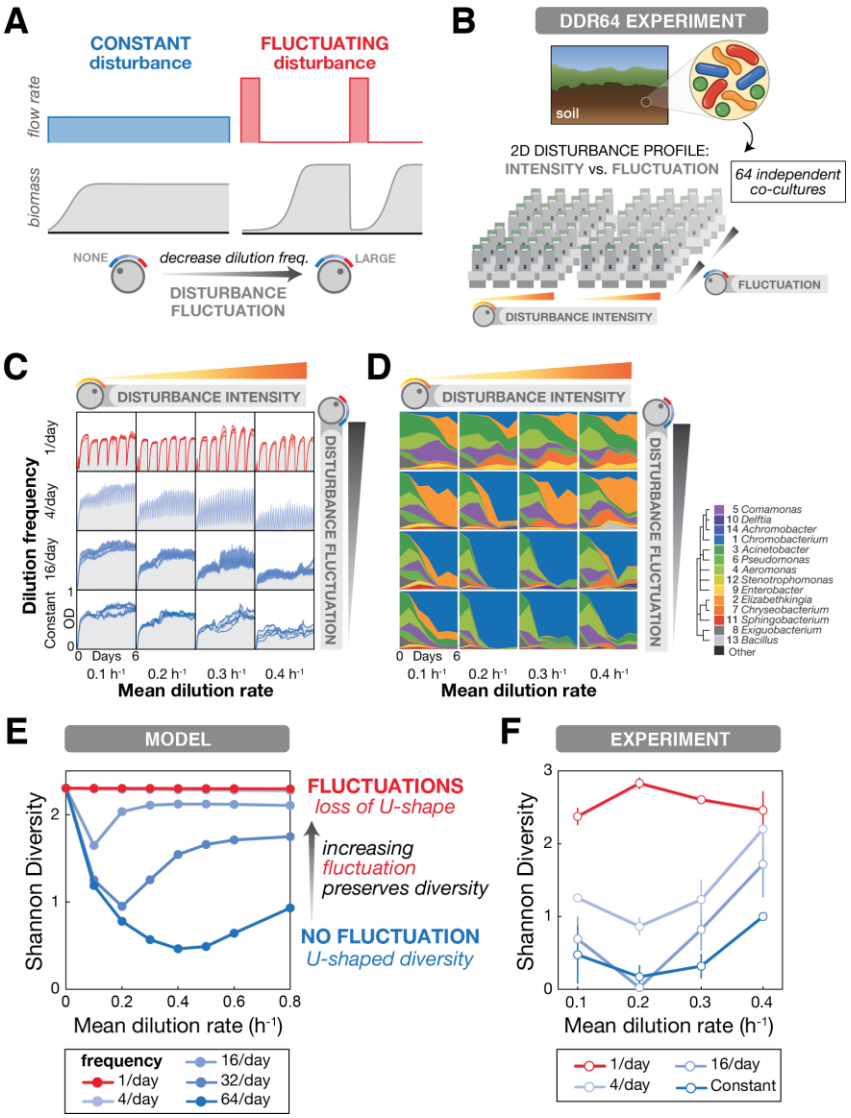

Fig. 3. Introducing environmental fluctuations weakens the U-shaped diversity curve and increases diversity levels in a microbial community. (A) Fluctuations in a disturbance over time cause fluctuations in biomass, and can be varied independently of the disturbance intensity. In continuous culture, fluctuations are achieved by aggregating dilution into discrete events while keeping mean dilution rate constant per day. **(B)** Schematic of the eVOLVER DDR64 experiment in which disturbance components (intensity and fluctuation) are varied independently. Samples of a soil-derived bacterial community were continuously cultured for 6 days across 64 eVOLVER bioreactors with varying mean dilution rate and dilution frequency. **(C)** Optical density traces for culture replicates in each condition show the dependence of biomass on disturbance. **(D)** Mean relative abundance of bacterial genera from replicate cultures, determined by 16S sequencing. Mean rank abundance is denoted by order, taxonomic similarity is denoted by color (see legend). **(E)** Mean Shannon diversity across 100 Monod consumer resource model simulations with varying mean dilution rate and dilution frequency show that the dependence of diversity on disturbance is fluctuation-dependent. **(F)** Mean Shannon diversity of Amplicon Sequence Variants from the DDR64 experiment vs. mean dilution rate and dilution frequencies. As in the simulations, fluctuations increase diversity and eliminate the U-shape. Bars in **E** and **F** denote standard error of the mean.

We hypothesized that tradeoffs in *r* & *K* growth parameters in the Monod model could lead to U-shaped diversity curves under varying disturbance intensities. Consider two species (A and B), competing for a single resource (**Fig. 4A**). If A has a small saturation constant *K*, it may outcompete species B at low resource levels, but it will lose at high resource levels if B has a higher maximum growth rate *r* (**Fig. 4A, left**). In the constant-disturbance conditions of a chemostat, the equilibrium resource concentration is proportionally related to dilution rate, such that the outcome of this competition depends entirely on dilution rate. Importantly, the opposite relationship may be observed when considering a different resource (**Fig. 4A, right**). These tradeoffs result in a 2-resource / 2-species system in which the Zero Net Growth Isoclines (ZNGIs) and resource consumption vectors flip as disturbance levels increase (**Fig. 4B**, Supplemental Note 1). In such a situation, which we term "niche flip," the outcomes of competition on either single resource flip as dilution rate increases. Critically, the resource consumption vectors outline a coexistence region when supplied with both resources; but as dilution rate increases, these vectors align temporarily, causing the coexistence region to disappear at some intermediate dilution rate (**Fig. 4B**). In systems of larger numbers of species and resources, *r*/*K* tradeoffs between pairs of species can drive exclusion events that co-occur, yielding U-shaped DDRs.

We next asked whether these tradeoffs could be experimentally observed in isolates from our continuous culture experiments. Our DDR experiments from Figs. 1 and 3 were performed in dilute Nutrient Broth, a non-defined complex medium with diverse nutrient sources (e.g. amino acids, peptides, nucleic acids). This complexity precludes definitive identification of any specific nutrients with *r*/*K* tradeoffs that drive the DDR observed experimentally. Nevertheless, we devised two experiments to look for evidence of possible *r*/*K* tradeoff mechanisms. First, we looked for tradeoffs within individual resources that might appear in the complex media. We measured the maximum growth rate for isolates grown on amino acid carbon sources in M9 minimal media in a plate reader. We found each resource to be optimally utilized by a different species, consistent with tradeoffs on different resources (**Fig. 4C,** Supplementary Note 1). Second, we looked for tradeoffs across different resources, prompted by our theoretical analysis that showed that *r/K* tradeoffs within resources are not required to obtain the U-shape (Supplementary Note 2, and figs. S1-4 & S18). The absence of a U-shape in the model requires a positive correlation between *r* and *r/K* in the complex media. We thus measured *r* and *K* values for bacterial isolates from the same soil-derived microbiome by tracking growth in varying concentrations of Nutrient Broth. We observed a range of *r*/*K* values with a negative correlation between *r* and *r/K*, consistent with the presence of *r/K* tradeoffs (**Fig. 4D** & fig. S17). These two experimental observations support our hypothesis that niche-flip could produce the U-shaped DDRs for the species and conditions used in our experiments.

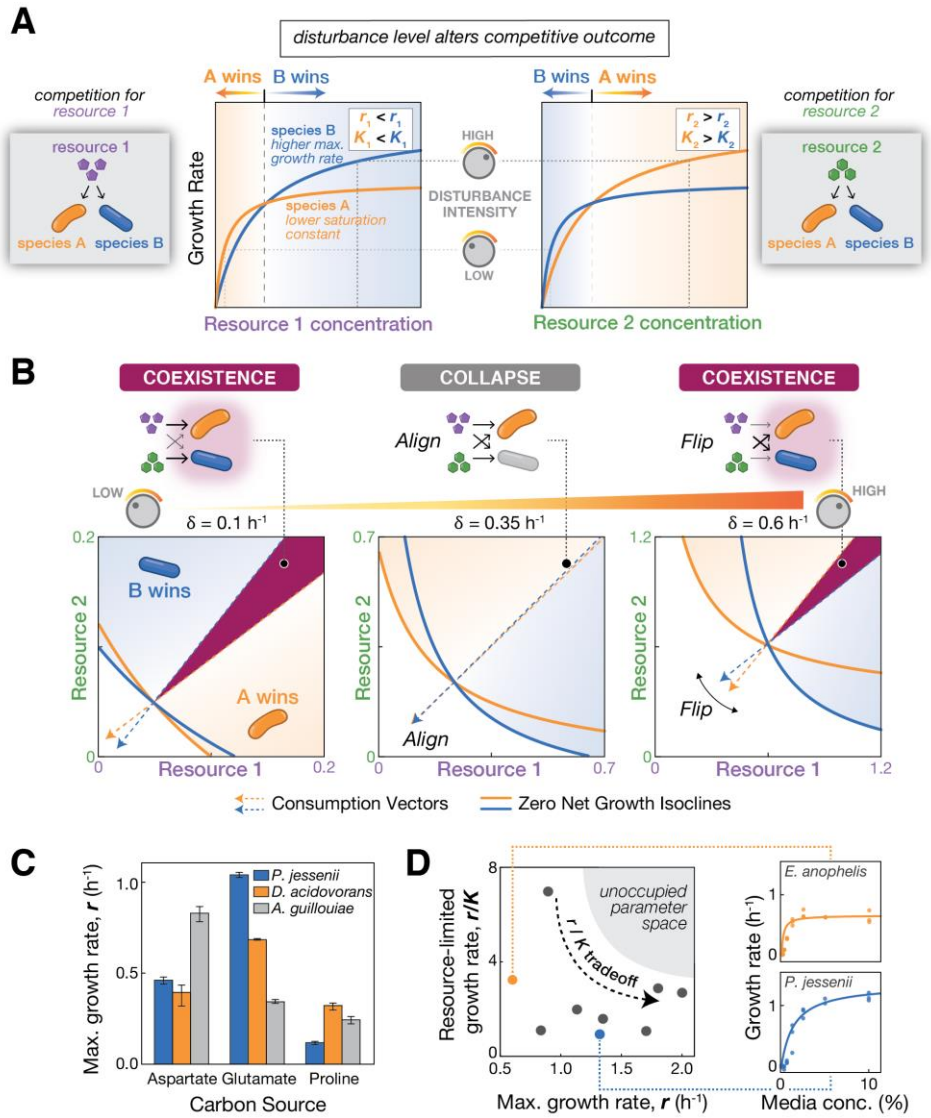

Fig. 4. Niche flip mechanism resulting from growth tradeoffs on multiple resources can give rise to U-shaped DDRs. (A) Monod growth curves with *r/K* tradeoffs change the outcome of competition depending on the resource and dilution rate. The species with a low saturation constant wins at low resource levels present at equilibrium in low dilution rates, whereas the species with a high maximum growth rate wins at high resource levels present at equilibrium in high dilution rates. **(B)** Flipping of both Zero Net Growth Isoclines (ZNGIs) and resource consumption vectors (defined as consumption by each species at the ZNGI intersection) in response to increasing dilution rates in a simulated 2-species / 2-resources co-culture. At intermediate dilution rates, consumption vectors align and the coexistence region collapses, reducing diversity relative to low/high dilution rates. The outcome of competition at the indicated resource supply point (black) is indicated at the top of each plot. **(C)** Isolates from the DDR64 experiment grown in M9 with different amino acids as sole carbon sources were found to have different maximum growth rates on different resources, consistent with coexistence in the niche flip mechanism. **(D)** *r/K* values for isolates from the DDR64 experiment indicate overall *r/K* tradeoffs in complex media. Strains were grown at various Nutrient Broth concentrations, and fit with Monod *r/K* parameters. No species were observed to have both favorable *r* (growth at high resource) and *r/K* (growth at low resource) values, indicating tradeoffs.

In this work, advances in automated continuous culture technology and next-generation sequencing enabled laboratory ecology studies to systematically dissect the role of environmental disturbance (intensity and fluctuation) with fine resolution at scale. We found replicable patterns in composition and diversity of a soil-derived microbial community across different disturbance regimes. Notably, we observed an unexpected U-shaped DDR under constant disturbance, and found that adding fluctuations to the disturbance removed this effect and increased community diversity. All of these results are well captured by a Monod consumer resource model, which subsequently led us to describe and propose a novel niche-flip mechanism that provides a plausible pathway for structuring these ecosystems. Taken together, these experimental and modeling results 1) provide new insight into how community assembly depends on environmental conditions and 2) demonstrate a role for environmental fluctuations in promoting diversity.

With further study and evaluation of underlying assumptions, the findings of this work may be extended to other systems. Though our experimental results were reproducible (figs. S11-12), it remains to be seen whether other species (microbial and macroscopic) and disturbance types (including asymmetric disturbances like toxins or heat shock) behave similarly. The generalizability of the niche-flip mechanism can be evaluated by reexamining the underlying assumptions and formulations of the Monod growth model. We have found that the U-shape is robust to alternative normalizations (fig. S18) and non-additive formulations of Monod growth on mixed substrates (*40*) (fig. S18). It remains to be seen whether niche-flip mechanisms could arise from non-resource-based models. It is plausible that similar growth tradeoffs arising in response to other disturbance-correlated features could lead to loss of coexistence at intermediate disturbance intensities. Therefore, niche flip could be a more general principle extending beyond relative growth non-linearities explored in this work to systems driven by dynamic abiotic stresses and/or storage effects (*41*–*44*).

Broadly, our results highlight that the structure of ecosystems and their response to perturbation is contextual. We demonstrated that increasing the disturbance intensity can increase, decrease, or have no effect on the diversity of a system, such that diverse classes of DDRs could emerge when only subsets of the parameter space are sampled (*14*–*16*, *33*). Critically however, we found these relationships to be predictable, rather than idiosyncratic. Additionally, this compositional complexity in the ecosystem is generated without invoking other organizing principles, such as spatial structure (*45*) or network structure (e.g. cross-feeding and antagonism) (*46*, *47*). If predictable response to perturbation depends on context, then designing predictable interventions to ecosystems (in medicine, agriculture, and conservation) will require the ability to measure and understand the environmental context. With the staggering amount of compositional data being generated with high throughput sequencing (*48*), inference of environmental context and design of robust ecological interventions may not be far off.

Materials and Methods

Lotka-Volterra Simulations

We simulated 10-species competitions with the Lotka-Volterra model:

$$\frac{1}{N_i}\frac{dN_i}{dt} = r_i\left(1 - \sum_{k=1}^{10}\alpha_{ik}N_j\right) \qquad Eqn.\,1$$

N_i represents the abundance of species i modified by its carrying capacity (we rescale the carrying capacities of all species to one), r_i represents its maximal growth rate, and α_{ik} represents inhibition of species i by species k. The model is parameterized such that $\alpha_{ii} = 1$.

Simulations mimicked experimental conditions as much as possible. Beginning with equal abundances of all 10 species, we integrated equations for a six-day period using the function ode45 in MATLAB. Species abundances were diluted during equally spaced 15-minute intervals by integrating a version of Eqn. 1 modified to include dilution:

$$\frac{1}{N_i}\frac{dN_i}{dt} = r_i\left(1 - \sum_{k=1}^{10}\alpha_{ik}N_k\right) - \delta \qquad Eqn.\,2$$

δ, the death/dilution rate, was calculated by distributing the mean dilution rate D (per hour) over equally spaced intervals of 15 minutes (per 1/4 hour) at a frequency f (per 24 hours):

$$\delta = \frac{1}{\left(\frac{1}{4}\right)hr} * \frac{D\left(\frac{1}{hr}\right)}{f\left(\frac{1}{24hr}\right)} = 96 * \frac{D}{f}\left(\frac{1}{hr}\right) \qquad Eqn.\,3$$

Frequency f of dilution ranged from 1 to 64 per day, and mean dilution rate D ranged from 0.1 to 0.8 per hour. Maximal growth rates r_i were randomly sampled from a normal distribution with mean 1 and standard deviation 0.1. This range was selected to roughly match measured growth rates of isolates on 0.1X Nutrient Broth (Fig. 4D). Competition coefficients α_{ik} were randomly sampled from a lognormal distribution with parameters $\mu = -0.7$ and $\sigma = 0.2$, which are the mean and standard deviation of the associated normal distribution. The mean of the lognormal distribution is $\exp\left(\mu + \frac{\sigma^2}{2}\right) = 0.51$ and the standard deviation is $\exp(2\mu) + \sigma^2(\exp(\sigma^2) - 1) = 0.1$. The competition coefficients were selected to match the diversity of the resource-explicit simulation results at the zero-dilution condition (see below). Other ranges of r_i and α_{ik} did not alter the DDR shape (fig. S8).

We simulated 100 competitions with randomly drawn parameters, across all dilution-frequency combinations. All 10 species began at equal abundances, and we used their final relative abundances p_i to calculate the Shannon diversity index ρ of each outcome:

$$\rho = \sum_{i=1}^{10} -p_i \ln p_i \qquad Eqn.\,4$$

In order to be counted, the abundance of a species p_i had to exceed a threshold of 0.0001. Finally, we took the average of the 100 values of ρ for each dilution-frequency combination to obtain average diversity.

Linear Consumer Resource Simulations

We simulated 10-species, seven-resource competitions with a linear resource concentration model:

$$\frac{1}{N_i}\frac{dN_i}{dt} = \sum_{j=1}^{7} r_{ij}c_j \qquad Eqn.\,5$$

N_i represents concentration of species i, r_{ij} its growth rate per unit resource on resource j, and c_j the concentration of resource j. Units of species and resources per volume are the same, because we assume that one unit of resource is fully converted into one unit of biomass; this assumption is equivalent to assuming the biomass yield is equal to one for all species, and therefore we do not include a yield parameter.

Similar to the Lotka-Volterra simulations, we integrated the dilution-modified equations over the same time period and range of frequencies and dilutions:

$$\frac{1}{N_i}\frac{dN_i}{dt} = \sum_{j=1}^{7} r_{ij}c_j - \delta \qquad Eqn.\,6$$

δ, as defined by Eqn. 3, is not only the dilution rate of cells, but also the influx of fresh resources at source concentration c_{jo}:

$$\frac{dc_j}{dt} = \delta\left(c_{jo} - c_j\right) - \sum_{i=1}^{10} N_i r_{ij} c_j \qquad Eqn.\,7$$

Simulations began with equal abundances of all species and resources ($c_{jo} = 1$), except for one resource, which had a slightly different supply concentration (c_{jo} =1.2), in order to move the resource supply point away from a unique central position. Growth rates per unit resource r_{ij} were randomly sampled from a normal distribution with mean 1 and standard deviation 0.1, and then normalized by dividing by the sum of growth rates for each species across all resources, $\sum_j^7 r_{ij}$. Other parameter ranges did not alter the DDR shape (fig. S9).

Monod Consumer Resource Simulations

We simulated 10-species, 7-resource competitions with a Monod resource model:

$$\frac{1}{N_i}\frac{dN_i}{dt} = \sum_{j=1}^{7} \frac{r_{ij}c_j}{K_{ij} + c_j} \qquad Eqn.\,8$$

The Monod constant, K_{ij}, is the concentration of resource j at which species i reaches its half-maximal growth rate on that resource. Similar to the linear resource concentration model (Eqns. 6-7), the model can be modified to include dilution:

$$\frac{1}{N_i}\frac{dN_i}{dt} = \sum_{j=1}^{7} \frac{r_{ij}c_j}{K_{ij}+c_j} - \delta \qquad Eqn.\,9$$

$$\frac{dc_j}{dt} = \delta(c_{jo} - c_j) - \sum_{i=1}^{10} \frac{N_i r_{ij} c_j}{K_{ij}+c_j} \qquad Eqn.\,10$$

We performed simulations using the same procedure described above. The Monod constants K_{ij} were randomly sampled from a uniform distribution: [0.001, 0.01]. The width of the selected range is consistent with the range of Monod constants measured on Nutrient Broth (Fig. 4D), and similar DDR shapes are generated with alternative parameter choices (fig. S18). Maximal growth rates r_{ij} were sampled and normalized as described above. To check whether the U-shaped DDR was preserved under variations of the Monod model, we performed other simulations (fig. S18).

First, we normalized maximal growth rates by dividing by the number of resources, rather than the sum of growth rates across all resources. The resulting diversity was more sensitive to disturbance intensity, causing diversity to decrease with mean dilution rate, but the U shape was preserved (fig. S18B).

Next, we employed a non-additive formulation of Monod growth on mixed substrates (*40*). In this formulation, the per-capita growth rate on multiple resources is a saturating function of Monod growth on individual resources, rather than a simple sum (as in Eqn. 10 above):

$$\frac{1}{N_i}\frac{dN_i}{dt} = \frac{\lambda_c \sum_{j=1}^{7} \frac{\phi_{ij}}{\lambda_c - \phi_{ij}}}{1 + \sum_{j=1}^{7} \frac{\phi_{ij}}{\lambda_c - \phi_{ij}}} \qquad Eqn.\,11$$

Here, $\phi_{ij} = \frac{r_{ij}c_j}{K_{ij}+c_j}$, which is the Monod growth of species i on resource j. The other parameter, λ_c, is the horizontal intercept in a plot of a species' catabolic enzyme expression as a function of its growth rate. For simplicity, we assumed λ_c to be equal for all species. Because the species consume resources non-additively in this model, the resources are also depleted non-additively:

$$\frac{dc_j}{dt} = -\sum_{i=1}^{10} \frac{N_i \phi_{ij}(\lambda_c - \phi_{ij})}{\lambda_c - \frac{1}{N_i}\frac{dN_i}{dt}} \qquad Eqn.\,12$$

We can write the dilution-modified model as follows (substituting $\lambda_c \gamma_i$ for per-capita growth of species i in the absence of dilution):

$$\frac{1}{N_i}\frac{dN_i}{dt} = \lambda_c \gamma_i - \delta \qquad Eqn.\,13$$

$$\frac{dc_j}{dt} = \delta\left(c_{jo} - c_j\right) - \sum_{i=1}^{10} \frac{N_i \phi_{ij}\left(\lambda_c - \phi_{ij}\right)}{\lambda_c - \lambda_c \gamma_i} \qquad Eqn.\,14$$

Simulating this model with values of λ_c ranging between 0.3 and 30 yielded DDRs similar to those of the summed Monod model, where the U shape was preserved (fig. S18C).

Diverging from the conditions of the experiment, we searched for alternative parameter ranges that could qualitatively alter the DDR. We found the model to be robust to increased simulation length (fig. S18D) and increased resource supply (fig. 18E). However, when reducing each of the resource supply concentrations, c_{jo}, by a divisive factor of 10, the U-shape was almost completely eliminated (except for a small effect at the highest dilution frequency, fig. S18F). This modification is equivalent to increasing Monod constants, K, by a multiplicative factor of 10, placing them closer to the range of resource supply concentration, which does not reflect our measurements (Fig. 4D) and is less biologically relevant. This extreme parameter range essentially changes the model choice, moving the growth dynamics closer to those of the linear consumer resource model.

Finally, we sought to determine whether other modifications to the summed Monod model would eliminate the U shape. First, we included the possibility of "specialist" species by widening the maximal growth rate sampling range. We randomly sampled r from a uniform distribution (0.1,1), before normalizing by dividing by the sum of growth rates for each species across all resources, $\sum_j^7 r_{ij}$, as before. The U shape was preserved (fig. S18G). Next, we eliminated r/K tradeoffs on all resources by sampling r and K as before, and then sorting them such that the species with the highest value of r also had the lowest value of K, and the next-highest and next-lowest, and so on, for each resource. The U shape was preserved (fig. S18H). Finally, we sampled K only once per resource, keeping it constant for all species on each resource. This modification eliminated the U shape (fig. S18I). For more discussion, see Supplementary Note 2.

Preparing Inoculum

2g of dirt from the Communications Lawn of Boston University (collected on 09/15/2018) was vortexed in 10 mL PBS + 200 ug/mL cycloheximide, then incubated in the dark at room temperature for 48 h. For pre-enrichment, 16 eVOLVER vials were prepared with 25 mL of 0.1X Nutrient Broth (NB) media (0.3 g/L yeast extract + 0.5 g/L peptone (Fisherbrand)) with 200 ug/mL cycloheximide, inoculated with 350 uL of PBS immersion, and grown for 18 h in eVOLVER at 25˚C. All 16 pre-enrichment cultures were mixed together to form the experiment inoculum. Aliquots in 15% glycerol were stored frozen at -80˚C.

Running eVOLVER Experiments

eVOLVER lines were sterilized using 10% bleach and ethanol (*35*, *36*), then autoclaved vials were loaded with 23 mL of 0.1X NB. Each vial was inoculated with 1 mL of inoculum, and

grown for 5 h at 25˚C with stirring prior to the first dilution disturbance. eVOLVER was operated in chemostat mode with 0.5 mL bolus size, with dilutions either evenly distributed over time (constant disturbance) or concentrated in fluctuation periods lasting 15 minutes. For these cultures, the flow rate during a fluctuation δ_f depended on the number of fluctuations per day f and mean dilution rate δ according to the following equation:

$$\delta_f = \frac{24 * \delta}{0.25 * f} \qquad Eqn.\ 15$$

At the end of each experiment, vials were flushed with media, and 10 optical density measurements were taken in eVOLVER to measure the biofilm levels.

Bottles and lines were routinely checked for contamination. This occurred to only a single vial of the experiment, which was excluded from statistical analysis. For the follow-up washout experiment, the glycerol stock inoculum was thawed at room temperature, 1 mL was inoculated into each vial, then the cultures were allowed to grow for 5.7 h prior to initiating disturbances. For the washout experiment, a software bug caused a few incorrectly executed dilution events; these vials were excluded from statistical analysis. Code required to execute these experiments will be available on Github (github.com/khalillab).

Sampling Cultures

At each timepoint, a 2 mL culture aliquot was removed from each vial with an extended length pipette tip.

For plating, 20 uL of the sample was used for a 10-fold serial dilution series, and 100 uL of diluted cultures at three concentrations were plated on 18 mL Nutrient Broth Agar plates (3 g/L yeast extract, 5 g/L peptone, 15 g/L agar (Fisherbrand)), which were grown at room temperature for 48-60 h, then imaged on an on an Epsom Perfection 550 scanner. Image analysis was performed with the aid of Cellprofiler 3.1.8 (*49*) and Cellprofiler Analyst 2.2.1 Classifier (*50*) tools.

For DNA extraction, the remainder of the sample was pelleted and frozen at -20˚C. 60-72 h after freezing, pellets were lysed at 37˚C for 1 h in 200 uL of lysozyme buffer (25mM Tris HCl pH 8.0, 2.5mM EDTA, 1% Triton X-100 with 20 mg/mL lysozyme (Fisher), prepared fresh daily). Lysates were processed using DNEasy Blood and Tissue Kit according to manufacturer specifications, eluted into 10 mM Tris buffer, and normalized to 5 ng/uL DNA based on measurements in a Qubit fluorometer.

Library Preparation and Sequencing

Briefly, we performed amplicon sequencing of the 16S v4 region based on established protocols (*18*). Primers prCM543 (TCGTCGGCAGCGTCAGATGTGTATAAGAGAC-AGGTGYCAGCMGCCGCGGTAA) and prCM544 (GTCTCGTGGGCTCGGAGATGTG-TATAAGAGACAGGGACTACNVGGGTWTCTAAT), adapted from EMP515F (*51*) and EMP806R (*52*) were used to isolate a 290 bp 16S v4 region, using Kapa Hifi ReadyMix polymerase and the following cycling conditions: (i) denaturation: 95°C for 5 min; (ii) amplification (25 cycles): 98°C for 20 s, 55°C for 15 s, 72°C for 1m ; (iii) elongation: 72°C for 5 min. For the negative control and biofilm samples, the number of cycles was increased to 35 to amplify from low biomass. Illumina NexteraXT primers (or equivalents) were used to form a final library 427 bp in length, with the following conditions: (i) denaturation: 95°C for 5 min; (ii)

amplification (8 cycles): 98°C for 20 s, 55°C for 15 s, 72°C for 1m ; (iii) elongation: 72°C for 10 min. DNA was purified with AMPure XP beads or SequalPrep plates, then samples were multiplexed in groups of 192 alongside control samples at a higher fraction, and spiked with PhiX or whole genome DNA libraries to a final concentration of 50% to increase sequence diversity. Library pools were sequenced at the Harvard Biopolymers Facility across five 250 bp paired end MiSeq v2 runs.

Sequencing Analysis

Samples were demultiplexed using the Illumina BaseSpace demultiplexer analysis tool. All subsequent bioinformatic analysis was performed in QIIME2 v2020.2 (*19*). Demultiplexed samples were dereplicated using DADA2 sample inference to tabulate Amplicon Sequencing Variants (ASVs) (*20*). Next, for qualitative description of composition, taxonomy (to the genus level) was assigned to each feature by alignment to the SILVA 132 database (*53*) using the taxa-barplot plugin. For quantitative analysis, samples with technical issues (e.g. contamination, low biomass, poor sequence quality, etc.) were removed and the remaining 698 samples were rarefied to 6840 reads. The fragment-insertion plugin was used to generate a rooted phylogenetic tree using the SEPP algorithm (*21*). The diversity plugin was used to calculate Shannon diversity, ASV richness, and weighted UniFrac distance (*54*), which was used to perform Principle Coordinate Analysis (PCoA).

Isolating Strains

Colonies from imaging plates for the inoculum and endpoint timepoints of the DDR64 and follow-up washout experiments were re-struck on NB agar plates, grown overnight in 0.1X NB media, and stored frozen at -80˚C in 15% glycerol. Primers prCM215 (CCATTGTAGCACGTG-TGTAGCC) and prCM216 (ACTCCTACGGGAGGCAGC) were used to amplify the v3-v7 16S region for Sanger sequencing and identification.

Growth Characterization of Isolates

Several strains with different taxonomic background were selected from the collection of isolates for further study. For measurement of *r*/*K* values, 9 strains were struck onto NB plates, and single colonies were grown to stationary phase overnight at 30˚C, then diluted to an OD600 of 0.001 in triplicate 200 uL cultures in dilute NB media (ranging from 0.1X to <0.0016X, plus a water-only negative control) in 96-well microplates grown in a Tecan spectrophotometer for 36 h at 30˚C, shaking, with lid on. Growth rates were fit to log transformed OD600 data, Lineweaver-Burke plots were constructed across media concentration, and Monod curves were fit to each species. Three strains that could grow in M9 defined minimal media were selected for characterization on different limiting resources. Strains were struck onto NB plates, and single colonies were grown to stationary phase overnight at 30˚C in carbon-limited M9 supplemented with aspartate, glutamate, or proline, then diluted and grown in microplates as above, with amino acid concentrations ranging from 10 mM to <0.16 mM, plus a no-carbon control. Due to limited growth on these media, optical densities at sub-saturating resource concentrations were below the limit of detection, so only maximum growth rate at 10 mM amino acid was reported.

Data Availability

Raw sequencing data will be available with a BioProject accession code. Plate images and all other experimental data are available upon request.

References and Notes:

1. D. Tilman, F. Isbell, J. M. Cowles, Biodiversity and Ecosystem Functioning. *Annu. Rev. Ecol. Evol. Syst.* **45**, 471–493 (2014).
2. O. Hoegh-Guldberg, J. F. Bruno, The impact of climate change on the world's marine ecosystems. *Science (80-.).* **328** (2010), pp. 1523–1528.
3. K. P. Lemon, G. C. Armitage, D. A. Relman, M. A. Fischbach, Microbiota-targeted therapies: An ecological perspective. *Sci. Transl. Med.* **4** (2012), pp. 137rv5-137rv5.
4. S. Widder, R. J. Allen, T. Pfeiffer, T. P. Curtis, C. Wiuf, W. T. Sloan, O. X. Cordero, S. P. Brown, B. Momeni, W. Shou, H. Kettle, H. J. Flint, A. F. Haas, B. Laroche, J. U. Kreft, P. B. Rainey, S. Freilich, S. Schuster, K. Milferstedt, J. R. Van Der Meer, T. Grobkopf, J. Huisman, A. Free, C. Picioreanu, C. Quince, I. Klapper, S. Labarthe, B. F. Smets, H. Wang, O. S. Soyer, S. D. Allison, J. Chong, M. C. Lagomarsino, O. A. Croze, J. Hamelin, J. Harmand, R. Hoyle, T. T. Hwa, Q. Jin, D. R. Johnson, V. de Lorenzo, M. Mobilia, B. Murphy, F. Peaudecerf, J. I. Prosser, R. A. Quinn, M. Ralser, A. G. Smith, J. P. Steyer, N. Swainston, C. E. Tarnita, E. Trably, P. B. Warren, P. Wilmes, Challenges in microbial ecology: Building predictive understanding of community function and dynamics. *ISME J.* **10** (2016), pp. 2557–2568.
5. J. H. Connell, Diversity in Tropical Rain Forests and Coral Reefs. *Science (80-.).* **199** (1978).
6. M. Huston, A General Hypothesis of Species Diversity. *Am. Nat.* **113**, 81–101 (1979).
7. P. Chesson, N. Huntly, The Role of Harsh and Fluctuating Conditions in the Dynamics of Ecological Communities. *Am. Nat.* (1997).
8. J. W. Fox, The intermediate disturbance hypothesis should be abandoned. *Trends Ecol. Evol.* **28**, 86–92 (2013).
9. C. Violle, Z. Pu, L. Jiang, Experimental demonstration of the importance of competition under disturbance. *Proc. Natl. Acad. Sci. U. S. A.* **107**, 12925–12929 (2010).
10. R. Levins, "Coexistence in a Variable Environment" (1979), (available at https://about.jstor.org/terms).
11. P. Chesson, Multispecies Competition in Variable Environments. *Theor. Popul. Biol.* **45**, 227–276 (1994).
12. A. D. Letten, M. K. Dhami, P. J. Ke, T. Fukami, Species coexistence through simultaneous fluctuation-dependent mechanisms. *Proc. Natl. Acad. Sci. U. S. A.* **115**, 6745–6750 (2018).
13. P. Chesson, Mechanisms of Maintenance of Species Diversity. *Annu. Rev. Ecol. Syst.* **31**, 343–366 (2000).
14. A. D. Miller, S. H. Roxburgh, K. Shea, How frequency and intensity shape diversity-disturbance relationships. *Proc. Natl. Acad. Sci. U. S. A.* **108**, 5643–8 (2011).
15. R. L. Mackey, D. J. Currie, The Diversity-Disturbance Relationship: Is It Generally Strong and Peaked? *Ecology*. **82**, 3479 (2001).
16. A. Randall Hughes, J. E. Byrnes, D. L. Kimbro, J. J. Stachowicz, Reciprocal relationships

and potential feedbacks between biodiversity and disturbance. *Ecol. Lett.* **10**, 849–864 (2007).

17. K. De Roy, M. Marzorati, P. Van den Abbeele, T. Van de Wiele, N. Boon, Synthetic microbial ecosystems: an exciting tool to understand and apply microbial communities. *Environ. Microbiol.* **16**, 1472–1481 (2014).

18. D. M. Gohl, P. Vangay, J. Garbe, A. MacLean, A. Hauge, A. Becker, T. J. Gould, J. B. Clayton, T. J. Johnson, R. Hunter, D. Knights, K. B. Beckman, Systematic improvement of amplicon marker gene methods for increased accuracy in microbiome studies. *Nat. Biotechnol.* **34**, 942–949 (2016).

19. E. Bolyen, J. R. Rideout, M. R. Dillon, N. A. Bokulich, C. C. Abnet, G. A. Al-Ghalith, H. Alexander, E. J. Alm, M. Arumugam, F. Asnicar, Y. Bai, J. E. Bisanz, K. Bittinger, A. Brejnrod, C. J. Brislawn, C. T. Brown, B. J. Callahan, A. M. Caraballo-Rodríguez, J. Chase, E. K. Cope, R. Da Silva, C. Diener, P. C. Dorrestein, G. M. Douglas, D. M. Durall, C. Duvallet, C. F. Edwardson, M. Ernst, M. Estaki, J. Fouquier, J. M. Gauglitz, S. M. Gibbons, D. L. Gibson, A. Gonzalez, K. Gorlick, J. Guo, B. Hillmann, S. Holmes, H. Holste, C. Huttenhower, G. A. Huttley, S. Janssen, A. K. Jarmusch, L. Jiang, B. D. Kaehler, K. Bin Kang, C. R. Keefe, P. Keim, S. T. Kelley, D. Knights, I. Koester, T. Kosciolek, J. Kreps, M. G. I. Langille, J. Lee, R. Ley, Y. X. Liu, E. Loftfield, C. Lozupone, M. Maher, C. Marotz, B. D. Martin, D. McDonald, L. J. McIver, A. V. Melnik, J. L. Metcalf, S. C. Morgan, J. T. Morton, A. T. Naimey, J. A. Navas-Molina, L. F. Nothias, S. B. Orchanian, T. Pearson, S. L. Peoples, D. Petras, M. L. Preuss, E. Pruesse, L. B. Rasmussen, A. Rivers, M. S. Robeson, P. Rosenthal, N. Segata, M. Shaffer, A. Shiffer, R. Sinha, S. J. Song, J. R. Spear, A. D. Swafford, L. R. Thompson, P. J. Torres, P. Trinh, A. Tripathi, P. J. Turnbaugh, S. Ul-Hasan, J. J. J. van der Hooft, F. Vargas, Y. Vázquez-Baeza, E. Vogtmann, M. von Hippel, W. Walters, Y. Wan, M. Wang, J. Warren, K. C. Weber, C. H. D. Williamson, A. D. Willis, Z. Z. Xu, J. R. Zaneveld, Y. Zhang, Q. Zhu, R. Knight, J. G. Caporaso, Reproducible, interactive, scalable and extensible microbiome data science using QIIME 2. *Nat. Biotechnol.* **37** (2019), pp. 852–857.

20. B. J. Callahan, P. J. McMurdie, M. J. Rosen, A. W. Han, A. J. A. Johnson, S. P. Holmes, DADA2: High-resolution sample inference from Illumina amplicon data. *Nat. Methods*. **13**, 581–583 (2016).

21. S. Janssen, D. McDonald, A. Gonzalez, J. A. Navas-Molina, L. Jiang, Z. Z. Xu, K. Winker, D. M. Kado, E. Orwoll, M. Manary, S. Mirarab, R. Knight, Phylogenetic Placement of Exact Amplicon Sequences Improves Associations with Clinical Information. *mSystems*. **3** (2018), doi:10.1128/msystems.00021-18.

22. J. Friedman, L. M. Higgins, J. Gore, Community structure follows simple assembly rules in microbial microcosms. *Nat. Ecol. Evol.* **1**, 0109 (2017).

23. O. S. Venturelli, A. V Carr, G. Fisher, R. H. Hsu, R. Lau, B. P. Bowen, S. Hromada, T. Northen, A. P. Arkin, Deciphering microbial interactions in synthetic human gut microbiome communities. *Mol. Syst. Biol.* **14** (2018), doi:10.15252/msb.20178157.

24. J. E. Goldford, N. Lu, D. Bajić, S. Estrela, M. Tikhonov, A. Sanchez-Gorostiaga, D. Segrè, P. Mehta, A. Sanchez, Emergent simplicity in microbial community assembly. *Science (80-.).* **361**, 469–474 (2018).

25. M. T. Mee, J. J. Collins, G. M. Church, H. H. Wang, Syntrophic exchange in synthetic microbial communities. *Proc. Natl. Acad. Sci. U. S. A.* **111**, E2149-56 (2014).

26. J. S. Chuang, Z. Frentz, S. Leibler, Homeorhesis and ecological succession quantified in synthetic microbial ecosystems. *Proc. Natl. Acad. Sci. U. S. A.* **116**, 14852–14861 (2019).

27. U. Sommer, Comparison between steady state and non-steady state competition: Experiments with natural phytoplankton. *Limnol. Oceanogr.* **30**, 335–346 (1985).

28. J. P. Grover, Dynamics of Competition in a Variable Environment: Experiments with Two Diatom Species. *Ecology*. **69**, 408–417 (1988).

29. S. M. Gibbons, M. Scholz, A. L. Hutchison, A. R. Dinner, J. A. Gilbert, M. L. Coleman, Disturbance Regimes Predictably Alter Diversity in an Ecologically Complex Bacterial System. *MBio*. **7**, e01372-16 (2016).

30. E. Santillan, H. Seshan, F. Constancias, D. I. Drautz-Moses, S. Wuertz, Frequency of disturbance alters diversity, function, and underlying assembly mechanisms of complex bacterial communities. *npj Biofilms Microbiomes*. **5**, 8 (2019).

31. S. M. Gibbons, M. Scholz, A. L. Hutchison, A. R. Dinner, J. A. Gilbert, M. L. Colemana, Disturbance regimes predictably alter diversity in an ecologically complex bacterial system. *MBio*. **7** (2016), doi:10.1128/mBio.01372-16.

32. C. I. Abreu, J. Friedman, V. L. Andersen Woltz, J. Gore, Mortality causes universal changes in microbial community composition. *Nat. Commun.* **10**, 1–9 (2019).

33. A. R. Hall, A. D. Miller, H. C. Leggett, S. H. Roxburgh, A. Buckling, K. Shea, Diversity-disturbance relationships: frequency and intensity interact. *Biol. Lett.* **8**, 768–71 (2012).

34. J. Monod, others, Technique, Theory and Applications of Continuous Culture. *Ann. Inst. Pasteur*. **79**, 390–410 (1950).

35. B. G. Wong, C. P. Mancuso, S. Kiriakov, C. J. Bashor, A. S. Khalil, Precise, automated control of conditions for high-throughput growth of yeast and bacteria with eVOLVER. *Nat. Biotechnol.* **36**, 614–623 (2018).

36. Z. J. Heins, C. P. Mancuso, S. Kiriakov, B. G. Wong, C. J. Bashor, A. S. Khalil, Designing automated, high-throughput, continuous cell growth experiments using eVOLVER. *J. Vis. Exp.* **2019**, e59652 (2019).

37. A. J. Lotka, A. J. Lotka, Elements of mathematical biology (1956).

38. D. Tilman, *Resource competition and community structure* (Princeton University Press, 1982).

39. R. MacArthur, Species packing and competitive equilibrium for many species. *Theor. Popul. Biol.* **1**, 1–11 (1970).

40. R. Hermsen, H. Okano, C. You, N. Werner, T. Hwa, A growth-rate composition formula for the growth of E. coli on co-utilized carbon substrates . *Mol. Syst. Biol.* **11**, 801 (2015).

41. A. L. W. Sears, P. Chesson, New methods for quantifying the spatial storage effect: An illustration with desert annuals. *Ecology*. **88**, 2240–2247 (2007).

42. A. L. Angert, T. E. Huxman, P. Chesson, D. L. Venable, Functional tradeoffs determine

species coexistence via the storage effect. *Proc. Natl. Acad. Sci. U. S. A.* **106**, 11641–11645 (2009).

43. J. Usinowicz, C. H. Chang-Yang, Y. Y. Chen, J. S. Clark, C. Fletcher, N. C. Garwood, Z. Hao, J. Johnstone, Y. Lin, M. R. Metz, T. Masaki, T. Nakashizuka, I. F. Sun, R. Valencia, Y. Wang, J. K. Zimmerman, A. R. Ives, S. J. Wright, Temporal coexistence mechanisms contribute to the latitudinal gradient in forest diversity. *Nature*. **550**, 105–108 (2017).

44. K. M. Hallinen, J. Karslake, K. B. Wood, Delayed antibiotic exposure induces population collapse in enterococcal communities with drug-resistant subpopulations. *Elife*. **9** (2020), doi:10.7554/eLife.52813.

45. S. Gude, E. Pinçe, K. M. Taute, A.-B. Seinen, T. S. Shimizu, S. J. Tans, Bacterial coexistence driven by motility and spatial competition. *Nature* (2020), doi:10.1038/s41586-020-2033-2.

46. M. T. Mee, J. J. Collins, G. M. Church, H. H. Wang, Syntrophic exchange in synthetic microbial communities. *Proc. Natl. Acad. Sci.* **111**, E2149–E2156 (2014).

47. E. D. Kelsic, J. Zhao, K. Vetsigian, R. Kishony, Counteraction of antibiotic production and degradation stabilizes microbial communities. *Nature*. **521**, 516–519 (2015).

48. L. R. Thompson, J. G. Sanders, D. McDonald, A. Amir, J. Ladau, K. J. Locey, R. J. Prill, A. Tripathi, S. M. Gibbons, G. Ackermann, J. A. Navas-Molina, S. Janssen, E. Kopylova, Y. Vázquez-Baeza, A. González, J. T. Morton, S. Mirarab, Z. Z. Xu, L. Jiang, M. F. Haroon, J. Kanbar, Q. Zhu, S. J. Song, T. Kosciolek, N. A. Bokulich, J. Lefler, C. J. Brislawn, G. Humphrey, S. M. Owens, J. Hampton-Marcell, D. Berg-Lyons, V. McKenzie, N. Fierer, J. A. Fuhrman, A. Clauset, R. L. Stevens, A. Shade, K. S. Pollard, K. D. Goodwin, J. K. Jansson, J. A. Gilbert, R. Knight, J. L. Agosto Rivera, L. Al-Moosawi, J. Alverdy, K. R. Amato, J. Andras, L. T. Angenent, D. A. Antonopoulos, A. Apprill, D. Armitage, K. Ballantine, J. Bárta, J. K. Baum, A. Berry, A. Bhatnagar, M. Bhatnagar, J. F. Biddle, L. Bittner, B. Boldgiv, E. Bottos, D. M. Boyer, J. Braun, W. Brazelton, F. Q. Brearley, A. H. Campbell, J. G. Caporaso, C. Cardona, J. L. Carroll, S. C. Cary, B. B. Casper, T. C. Charles, H. Chu, D. C. Claar, R. G. Clark, J. B. Clayton, J. C. Clemente, A. Cochran, M. L. Coleman, G. Collins, R. R. Colwell, M. Contreras, B. B. Crary, S. Creer, D. A. Cristol, B. C. Crump, D. Cui, S. E. Daly, L. Davalos, R. D. Dawson, J. Defazio, F. Delsuc, H. M. Dionisi, M. G. Dominguez-Bello, R. Dowell, E. A. Dubinsky, P. O. Dunn, D. Ercolini, R. E. Espinoza, V. Ezenwa, N. Fenner, H. S. Findlay, I. D. Fleming, V. Fogliano, A. Forsman, C. Freeman, E. S. Friedman, G. Galindo, L. Garcia, M. A. Garcia-Amado, D. Garshelis, R. B. Gasser, G. Gerdts, M. K. Gibson, I. Gifford, R. T. Gill, T. Giray, A. Gittel, P. Golyshin, D. Gong, H. P. Grossart, K. Guyton, S. J. Haig, V. Hale, R. S. Hall, S. J. Hallam, K. M. Handley, N. A. Hasan, S. R. Haydon, J. E. Hickman, G. Hidalgo, K. S. Hofmockel, J. Hooker, S. Hulth, J. Hultman, E. Hyde, J. D. Ibáñez-Álamo, J. D. Jastrow, A. R. Jex, L. S. Johnson, E. R. Johnston, S. Joseph, S. D. Jurburg, D. Jurelevicius, A. Karlsson, R. Karlsson, S. Kauppinen, C. T. E. Kellogg, S. J. Kennedy, L. J. Kerkhof, G. M. King, G. W. Kling, A. V. Koehler, M. Krezalek, J. Kueneman, R. Lamendella, E. M. Landon, K. Lanede Graaf, J. LaRoche, P. Larsen, B. Laverock, S. Lax, M. Lentino, I. I. Levin, P. Liancourt, W. Liang, A. M. Linz, D. A. Lipson, Y. Liu, M. E. Lladser, M. Lozada, C. M. Spirito, W. P. MacCormack, A. MacRae-Crerar, M. Magris, A. M. Martín-Platero, M. Martín-Vivaldi, L. M. Martínez, M.

Martínez-Bueno, E. M. Marzinelli, O. U. Mason, G. D. Mayer, J. M. McDevitt-Irwin, J. E. McDonald, K. L. McGuire, K. D. McMahon, R. McMinds, M. Medina, J. R. Mendelson, J. L. Metcalf, F. Meyer, F. Michelangeli, K. Miller, D. A. Mills, J. Minich, S. Mocali, L. Moitinho-Silva, A. Moore, R. M. Morgan-Kiss, P. Munroe, D. Myrold, J. D. Neufeld, Y. Ni, G. W. Nicol, S. Nielsen, J. I. Nissimov, K. Niu, M. J. Nolan, K. Noyce, S. L. O'Brien, N. Okamoto, L. Orlando, Y. O. Castellano, O. Osuolale, W. Oswald, J. Parnell, J. M. Peralta-Sánchez, P. Petraitis, C. Pfister, E. Pilon-Smits, P. Piombino, S. B. Pointing, F. J. Pollock, C. Potter, B. Prithiviraj, C. Quince, A. Rani, R. Ranjan, S. Rao, A. P. Rees, M. Richardson, U. Riebesell, C. Robinson, K. J. Rockne, S. M. Rodriguezl, F. Rohwer, W. Roundstone, R. J. Safran, N. Sangwan, V. Sanz, M. Schrenk, M. D. Schrenzel, N. M. Scott, R. L. Seger, A. Seguinorlando, L. Seldin, L. M. Seyler, B. Shakhsheer, G. M. Sheets, C. Shen, Y. Shi, H. Shin, B. D. Shogan, D. Shutler, J. Siegel, S. Simmons, S. Sjöling, D. P. Smith, J. J. Soler, M. Sperling, P. D. Steinberg, B. Stephens, M. A. Stevens, S. Taghavi, V. Tai, K. Tait, C. L. Tan, N. Taş, D. L. Taylor, T. Thomas, I. Timling, B. L. Turner, T. Urich, L. K. Ursell, D. Van Der Lelie, W. Van Treuren, L. Van Zwieten, D. Vargas-Robles, R. V. Thurber, P. Vitaglione, D. A. Walker, W. A. Walters, S. Wang, T. Wang, T. Weaver, N. S. Webster, B. Wehrle, P. Weisenhorn, S. Weiss, J. J. Werner, K. West, A. Whitehead, S. R. Whitehead, L. A. Whittingham, E. Willerslev, A. E. Williams, S. A. Wood, D. C. Woodhams, Y. Yang, J. Zaneveld, I. Zarraonaindia, Q. Zhang, H. Zhao, A communal catalogue reveals Earth's multiscale microbial diversity. *Nature*. **551**, 457–463 (2017).

49. M. R. Lamprecht, D. M. Sabatini, A. E. Carpenter, CellProfiler^{TM}: Free, versatile software for automated biological image analysis. *Biotechniques*. **42**, 71–75 (2007).

50. M.-A. Bray, M. S. Vokes, A. E. Carpenter, Using CellProfiler for Automatic Identification and Measurement of Biological Objects in Images, doi:10.1002/0471142727.mb1417s109.

51. A. Apprill, S. McNally, R. Parsons, L. Weber, Minor revision to V4 region SSU rRNA 806R gene primer greatly increases detection of SAR11 bacterioplankton. *Aquat. Microb. Ecol.* **75**, 129–137 (2015).

52. A. E. Parada, D. M. Needham, J. A. Fuhrman, Every base matters: Assessing small subunit rRNA primers for marine microbiomes with mock communities, time series and global field samples. *Environ. Microbiol.* **18**, 1403–1414 (2016).

53. C. Quast, E. Pruesse, P. Yilmaz, J. Gerken, T. Schweer, P. Yarza, J. Rg Peplies, F. O. Glö Ckner, The SILVA ribosomal RNA gene database project: improved data processing and web-based tools, doi:10.1093/nar/gks1219.

54. C. Lozupone, M. E. Lladser, D. Knights, J. Stombaugh, R. Knight, UniFrac: An effective distance metric for microbial community comparison. *ISME J.* **5** (2011), pp. 169–172.

55. J. Kehe, A. Kulesa, A. Ortiz, C. M. Ackerman, S. G. Thakku, D. Sellers, S. Kuehn, J. Gore, J. Friedman, P. C. Blainey, Massively parallel screening of synthetic microbial communities. *Proc. Natl. Acad. Sci. U. S. A.* **116**, 12804–12809 (2019).

56. M. M. Villa, R. J. Bloom, J. D. Silverman, H. K. Durand, S. Jiang, A. Wu, S. Huang, L. You, L. A. David, High-throughput isolation and culture of human gut bacteria with droplet microfluidics. *bioRxiv*, 630822 (2019).

Acknowledgments: We thank members of the Gore and Khalil groups for helpful discussions. We thank S. Boswell for sequencing advice, M. Springer and J. Galagan for reagents and equipment used in library preparation, and the Harvard Biopolymers Facility for their services. **Funding:** This work was supported by DARPA BRICS grants HR001115C0091 (J.G. and A.S.K.) and HR001117S0029 (A.S.K.), Simons Foundation grant 542385 (J.G.), and NIH grants R01GM102311 (J.G.) and R01EB027793 (A.S.K.). A.S.K. also acknowledges funding from the NIH Director's New Innovator Award (1DP2AI131083-01) and NSF CAREER Award (MCB-1350949). **Author contributions:** C.P.M., J.G. and A.S.K. conceived the study. C.P.M. performed all experiments and sequencing analysis. H.L. and C.I.A. performed theoretical modeling. All authors analyzed results. J.G. and A.S.K. oversaw the study. All authors wrote the manuscript. **Competing interests:** A.S.K. is co-founder of Fynch Biosciences, a manufacturer of eVOLVER hardware. **Data and materials availability:** All sequencing data is being deposited in the Sequence Read Archive (SRA) and will be accessible with a BioProject accession code (Submission number: SUB7786275). Other datasets generated and analyzed during the current study are available upon request from the corresponding author. Computer code used to run eVOLVER experiments and for theoretical modeling is available at github.com/khalillab.

Supplementary Materials:

Supplementary Text

Figures S1-S18

References (*49*–*56*)